© 2016. Published by The Company of Biologists Ltd | Journal of Experimental Biology (2016) 219, 3082-3090 doi:10.1242/jeb.134536

RESEARCH ARTICLE

# Experimental tests of planar strain theory for predicting bone cross-sectional longitudinal and shear strains

**Kari A. Verner[1], Michael Lehner[1], Luis P. Lamas[2] and Russell P. Main[1,3,*]**

## ABSTRACT

Understanding of the diversity of skeletal loading regimes in vertebrate long bones during locomotion has been significantly enhanced by the application of planar strain theory (PST) to *in vivo* bone strain data. PST is used to model the distribution of longitudinal strains normal to the bone's transverse cross-section and the location of the neutral axis of bending. To our knowledge, the application of this theory to skeletal biomechanics has not been experimentally validated. We evaluated the accuracy of PST using strain measurements from emu tibiotarsi instrumented with four strain gauges and loaded in *ex vivo* four-point bending. Using measured strains from three-gauge combinations, PST was applied to predict strain values at a fourth gauge's location. Experimentally measured and predicted strain values correlated linearly with a slope near 1.0, suggesting that PST accurately predicts longitudinal strains. Additionally, we assessed the use of PST to extrapolate shear strains to locations on a bone not instrumented with rosette strain gauges. Guineafowl tibiotarsi were instrumented with rosette strain gauges and *in vivo* longitudinal and shear strains were measured during treadmill running. Individual-specific and sample-mean ratios between measured longitudinal strains from the medial and posterior bone surfaces were used to extrapolate posterior-site shear strain from shear strains measured on the medial surface. Measured and predicted shear strains at the posterior gauge site using either ratio showed trends for a positive correlation between measured and predicted strains, but the correlation did not equal 1.0 and had a non-zero intercept, suggesting that the use of PST should be carefully considered in the context of the goals of the study and the desired precision for the predicted shear strains.

**KEY WORDS: Skeletal biomechanics, Avian locomotion, Tibiotarsus**

## INTRODUCTION

The application of methods for predicting the distribution of longitudinal strains normal to a long bone's transverse cross-section, and the location of the neutral axis of bending in the cross-section, has significantly enhanced our understanding of the diversity of *in vivo* skeletal loading regimes found in vertebrate long bones during locomotion. Surface strain gauge measurements are used frequently to characterize 'typical' bone tissue strains during locomotion *in vivo*, as well as artificially induced *ex vivo* strains, in order to estimate safety factors and mechanical properties in a large variety of animals and bones (Biewener and Dial, 1995; Blob and Biewener, 1999; Butcher et al., 2008, 2011; Main and Biewener, 2007; Rubin and Lanyon, 1985). Limitations of bone size and surgical surface availability often restrict the possible locations for gauge implantation as well as the type and size of the strain gauge used (single element versus rosette gauge). As a result, it is often difficult to place gauges at the exact locations of maximum strain, even if these locations can be estimated *a priori*. However, if three strain gauges can be distributed around the diaphyseal cortex, planar strain theory (PST) can be used to estimate the cross-sectional strain distribution, the sites of maximum tensile and minimum compressive strains, and the location of the neutral axis of bending (Biewener, 1992; Carter et al., 1981; Lieberman et al., 2004). Although this technique is used frequently in *in vivo* skeletal biomechanics studies, its accuracy for this application and the possible effect of gauge distribution around the diaphysis have not been validated experimentally to our knowledge.

Measures of shear strain, which are dependent upon the magnitudes and orientations of the principal strains in the bone, describe the off-axis loading of the bone including long-axis torsion, and can be calculated directly when a rosette gauge is attached to the bone's surface (Biewener, 1992; Carter, 1978). While these direct measures of bone tissue shear are only valid at the location of the rosette gauge, there is interest in determining maximum shear strains around a bone's circumference, which may not coincide with the location of the attached rosette strain gauge. Some studies have applied PST-based longitudinal strain ratios to shear strain measures at one location to estimate shear strains at the PST-determined maximum longitudinal strain location on the bone (Blob and Biewener, 1999; Butcher et al., 2008). In this approach, an average longitudinal strain ratio was determined between the longitudinal strain values measured at a rosette gauge site and the site of maximum compressive strain on the bone, determined using PST from all animals in the study. This average longitudinal strain ratio was then applied to the shear strain measured at the rosette gauge for each animal to predict each individual's maximal shear strains. In this way, the estimated peak shear strain in the bone would always be larger than the measured shear strain, ensuring that any safety factor determined based upon the *in vivo* strain data would not be artificially inflated by using submaximal shear strain values. This approach requires the assumptions that shear strains increase in proportion to longitudinal strains around the bone's cortex, and that maximum shear strains occur at the same location as maximum longitudinal strains. These assumptions have not been experimentally validated in published literature. While the equation for shear strain does include a component of the longitudinal strain, it also depends on off-axis strain values and principal strain angles that do not necessarily change in a predictable way around a bone cross-section, but could have a large impact on shear strain values.

[1]Weldon School of Biomedical Engineering, Purdue University, West Lafayette, IN 47907, USA. [2]Faculdade de Medicina Veterinária, Universidade de Lisboa, Pólo da Ajuda, Lisboa 1300-477, Portugal. [3]Department of Basic Medical Sciences, College of Veterinary Medicine, Purdue University, West Lafayette, IN 47907, USA.

*Author for correspondence (rmain@purdue.edu)

R.P.M., 0000-0003-1967-1122

**Received 9 November 2015; Accepted 22 July 2016**



Journal of Experimental Biology

Journal of Experimental Biology (2016) 219, 3082-3090 doi:10.1242/jeb.134536

One goal of this paper was to evaluate the accuracy of PST in predicting cross-sectional strains given different strain gauge distributions around the cross-section of the bone. To address this goal, we attached four strain gauges around the midshafts of adult emu tibiotarsi (TBTs) and loaded the instrumented bones in *ex vivo* four-point bending. Using combinations of experimentally measured strain values from three of the four gauges to create planar strain reconstructions for the midshaft cross-sections, we determined the predicted strain value at the location of the fourth gauge and compared it with the corresponding experimentally measured value. We hypothesized that regardless of the distribution of the gauges around the midshaft used for calculations, reconstructed strains would not be significantly different from the measured strains.

Our second goal was to evaluate the use of longitudinal strain ratios for extrapolating shear strains measured from a rosette strain gauge to positions on the bone cross-section that were not strain gauge instrumented or were instrumented with a single element gauge incapable of measuring shear strain. To this end, *in vivo* longitudinal and shear strains were measured using three rosette strain gauges on the posterior, anterior and medial midshaft surfaces of guineafowl TBTs at a specific point in the stride during treadmill running. With these data we tested the assumptions made when using longitudinal strain ratios relating the longitudinal strains at two gauge sites for predicting shear strain from one rosette gauge site to another. Like similar attempts to do this previously (Blob and Biewener, 1999; Butcher et al., 2008), this prediction makes the assumption that shear strains change in proportion to longitudinal strains across the cross-section. While our methods require shear strain predictions to be extrapolated to locations on the bone surface that may not coincide with the maximum longitudinal strain, our extrapolations to sites of empirically measured shear strains allow us to experimentally test the predictions. Through these analyses, we sought to evaluate the accuracy of using a linear model based upon longitudinal strain measures for predicting shear strains in long bones.

## MATERIALS AND METHODS

### PST validation

The TBTs of emu [*Dromaius novaehollandiae* (Latham 1790)] were used in four-point bending tests to validate PST for animal long bones. The TBTs used in this study ($N$=5) were from the non-instrumented right limbs of birds used in a prior *in vivo* bone strain study (Main and Biewener, 2007), which were dissected from the body and frozen at −20°C. At time of the study, the birds ranged in age from 36 to 75 weeks of age (62±18 weeks, mean±1 s.d.) and in mass from 29 to 52 kg (40.6±11.4 kg). At a later date, each TBT was thawed, cleaned of soft tissue and muscle, wrapped in water-soaked paper towels, wrapped in a plastic bag, and re-frozen at −20°C. Prior to the testing conducted for this study, the bones were individually thawed, aligned using a custom-made alignment frame and fixed in machined aluminium pots using a commercial fast-drying cement (Body Filler, 3M, Saint Paul, MN, USA). The proximal and distal ends of the bone were embedded such that 50% of bone length centered at the midshaft remained exposed. Exposed bone was kept moist during potting and between mechanical tests using saline-soaked paper towels. Once the cement hardened, the potted bones were refrozen at −20°C. At a later date, the bones were thawed for the final time to conduct strain gauge implantation and mechanical testing. Thus, all bones went through three freeze–thaw cycles prior to mechanical testing. Once thawed, three rosette strain gauges (FRA-2-11, Tokyo Sokki Kekyujo Co., Ltd, Tokyo, Japan) and one single-element gauge (FLA-3-11) were attached around the circumference of the bone's midshaft (Fig. 1). A 1.5 $cm^2$ region of periosteum was scraped away at each gauge attachment site using a periosteal elevator. The bone surface was defatted and dried using 2-butanone (Sigma-Aldrich, St Louis, MO, USA) and the gauges bonded to each site using a self-catalyzing cyanoacrylate adhesive (DURO Superglue, Loctite, Westlake, OH, USA). Rosette strain gauges were attached to anterior, posterior and medial surfaces and a single element gauge was attached to an anterior–medial surface at the bone's midshaft with a goal of spacing the gauges as evenly around the cross-section as possible while respecting any bone surface limitations. The gauges were oriented so that the central element of each gauge was aligned with the long axis of the bone. Gauge lead wires were soldered to a microconnector (4-103240-0, Digi-Key, Thief River Falls, MN, USA) that was plugged into a 1 m shielded cable (NMuF 6/30-404655, Coonerwire, Chatsworth, CA, USA), to convey raw strain signals to Vishay amplifiers (2110B, Vishay Precision Group, City of Industry, CA, USA). During testing, amplified strain signals were sampled at 100 Hz through an A/D converter and converted to microstrain (με, strain×$10^6$) in the manufacturer's software (Labchart7, ADInstruments, Dunedin, New Zealand).

Each instrumented emu TBT was loaded over its linear elastic range (i.e. not to failure) in four-point bending. A −10 N pre-load was applied to hold the specimen in place and to maintain equal distribution of load among the four contact points. Five triangular waveform cycles of preconditioning from −10 to −20 N were applied at a load rate of 0.25 mm $s^{-1}$, immediately followed by 10 triangular waveform load–unload cycles from −10 to −175 N compressive load at 0.25 mm $s^{-1}$ to induce an average peak bending moment of −9.63 N m at the time of maximum applied load (Table 1, Fig. 2). Each surface of the bone was loaded in turn in compression by placing the surfaces sequentially 'face-up' in the load fixture in the following order: anterior, medial, posterior and lateral. The applied load from the load cell and bone strain readings from the four strain gauges were collected synchronously. The length:width aspect ratio of the tested bone region was approximately 18:1.

Following the four-point bending tests, planar strain analyses were conducted using different three-gauge combinations in order to test the accuracy of this method for modeling load-induced strains against the measured strain in the fourth gauge. Using a custom-

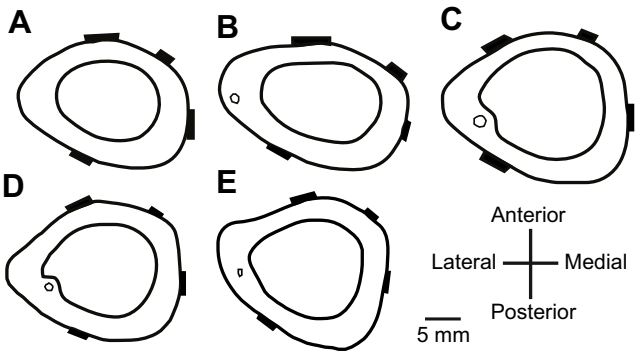


**Fig. 1. Cross-sections for each emu tibiotarsus (TBT) included in this study.** The strain gauge positions are indicated with black rectangles for the five TBT (A–E). Gauge coverage percentage was measured as the distance around the circumference of the gauge for three consecutive gauges used for the prediction (i.e. for posterior site prediction, circumference between anterior, anterior–medial and medial gauge locations was measured) over the total circumference.

Journal of Experimental Biology (2016) 219, 3082-3090 doi:10.1242/jeb.134536

**Table 1. Emu subject data and four-point bending test parameters**

| Animal | Age (weeks) | Mass (kg) | TBT length (cm) | TBT AP diameter (mm) | TBT ML diameter (mm) | Four-point bending test parameters | | | | |
|---|---|---|---|---|---|---|---|---|---|---|
| | | | | | | Inner span distance (m) | Outer span distance (m) | *a* (m) | Peak load (N) | Moment applied (N m) |
| A | 36 | 27.4 | 42 | 19.4 | 23.7 | 0.256 | 0.452 | 0.098 | −175 | −8.58 |
| B | 48 | 30.0 | 44 | 21.8 | 24.9 | 0.234 | 0.452 | 0.109 | −175 | −9.54 |
| C | 74 | 43.1 | 43.5 | 25.8 | 28.6 | 0.233 | 0.460 | 0.114 | −175 | −9.93 |
| D | 75 | 50.9 | 43 | 24.8 | 29.2 | 0.255 | 0.470 | 0.108 | −175 | −9.41 |
| E | 75 | 51.7 | 43 | 24.5 | 27.8 | 0.200 | 0.445 | 0.123 | −175 | −10.72 |

TBT, tibiotarsus; AP, antero-posterior; ML, medio-lateral; *a*, horizontal distance between the top and bottom load points.

written MATLAB (Mathworks, Natick, MA, USA) program, the raw longitudinal strain values were zeroed by subtracting the average strain in each channel measured prior to the upper load fixture contacting the sample. Then, a single cross-sectional slice from a CT scan (0.63 mm in-plane resolution, GE Lightspeed VCT, GE Healthcare, Purdue Veterinary Teaching Hospital) of each bone with all four gauges visible was imported into MATLAB and the location of each gauge manually selected in the program. In each bending orientation, the longitudinal strains were predicted for each gauge location in turn using the strain measures from the three other gauges and equations previously described for calculating the distribution of longitudinal strains normal to the bone's cross-section (Biewener, 1992; Carter et al., 1981):

$$\begin{aligned} \varepsilon_1 &= A\,x_1 + B\,y_1 + C \\ \varepsilon_2 &= A\,x_2 + B\,y_2 + C \\ \varepsilon_3 &= A\,x_3 + B\,y_3 + C. \end{aligned} \quad (1)$$

Eqn 1 represents the equations used for PST predictions. $x$ and $y$ are the 2D coordinates of the strain gauge position on the bone cross-section. Strain ($\varepsilon$) is the strain measured at the corresponding gauge site. By solving the set of three equations, the coefficients $A$, $B$ and $C$ can be determined. Once those coefficients are known, the strain at any location across the bone's cross-section can be determined. For each gauge, peak and predicted strains were determined for the final five load cycles for each bending direction and then averaged, resulting in a measured strain and predicted strain for each gauge on each bone. Thus, in Fig. 3, each data point represents a mean value for measured and predicted strains for five cycles of loading for each bone. Calculated versus measured strains were plotted for the four gauge locations in each of the four bending directions for the $N$=5 bones tested, such that each bone is represented by four data points (once for each bending direction) in Fig. 3. A least-squares linear regression was fitted to the predicted versus measured strain data for each strain gauge location for all birds (20 data points: 5 birds with 4 strain gauge predictions each) across the four bending directions to determine the slope between the measured and calculated strain values. Ninety-five percent confidence intervals (CI) were calculated to determine whether the slope of the regression was significantly different from unity.

We also quantitatively characterized the extent of the circumferential coverage of the strain gauges for the different three-gauge combinations by measuring the length along the bone's circumference between the three successive gauges for each combination. This was achieved by manually tracing the total circumference of the bone and the length of the perimeter between the center of the gauge foil for each of the three successive gauges for each combination from the CT scan images (ImageJ, National Institutes of Health, Bethesda, MD, USA). Coverage percentages were averaged for all five animals for each of the four three-gauge combinations.

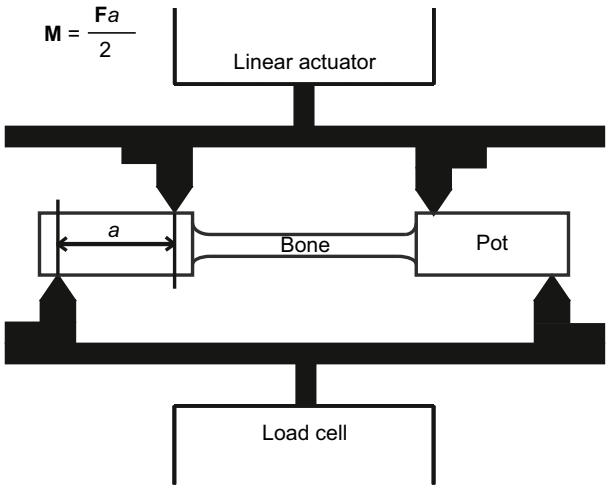


**Fig. 2. Schematic diagram of the four-point bending apparatus.** The load points were adjusted horizontally for each bone to maximize the bending moment. The equation shown calculates the bending moment the bone will experience, where **M** is the bending moment, **F** is the total force applied from the top load points, and *a* is the horizontal distance between the top and bottom load points.

### Extrapolation of PST to shear strains

Male french guineafowl [*Numida meleagris* (Linnaeus)] were used to evaluate the validity of using the relationship between planar strains at two cortical bone sites in a cross-section to determine shear strains at a bone site remote to the location of a rosette strain gauge. All birds used were obtained from a commercial farm (JM Hatchery, New Holland, PA, USA; $N$=5) as hatchlings and raised at Purdue University in an indoor enclosure with free access to game bird feed and water until they were used in the study (age: 21.6±0.9 weeks, mass: 2.72±0.27 kg). All surgical and experimental procedures followed protocols approved by the Purdue University IACUC (PACUC Protocol no. 1310000977).

Aseptic surgery was conducted to attach strain gauges to each bird's left TBT. The birds were induced for surgery through mask inhalation of isoflurane (5%), and maintained at a surgical anesthetic plane with 2–4% isoflurane at a 1 l min$^{-1}$ $O_2$ flow rate. Breathing and heart rate were monitored throughout surgery, and anesthesia adjusted as necessary. To attach strain gauges to the midshaft of the TBT, incisions were made at the lateral border of the synsacrum and on the medial side of the TBT at the midshaft. Three rosette strain gauges (FRA-1-11, Tokyo Sokki Kenkyujo Co., Ltd, Tokyo, Japan) and their lead wires were passed subcutaneously from the incision at the sacrum to the incision at the TBT midshaft. After retracting the overlying muscles to expose anterior, posterior

Journal of Experimental Biology (2016) 219, 3082-3090 doi:10.1242/jeb.134536

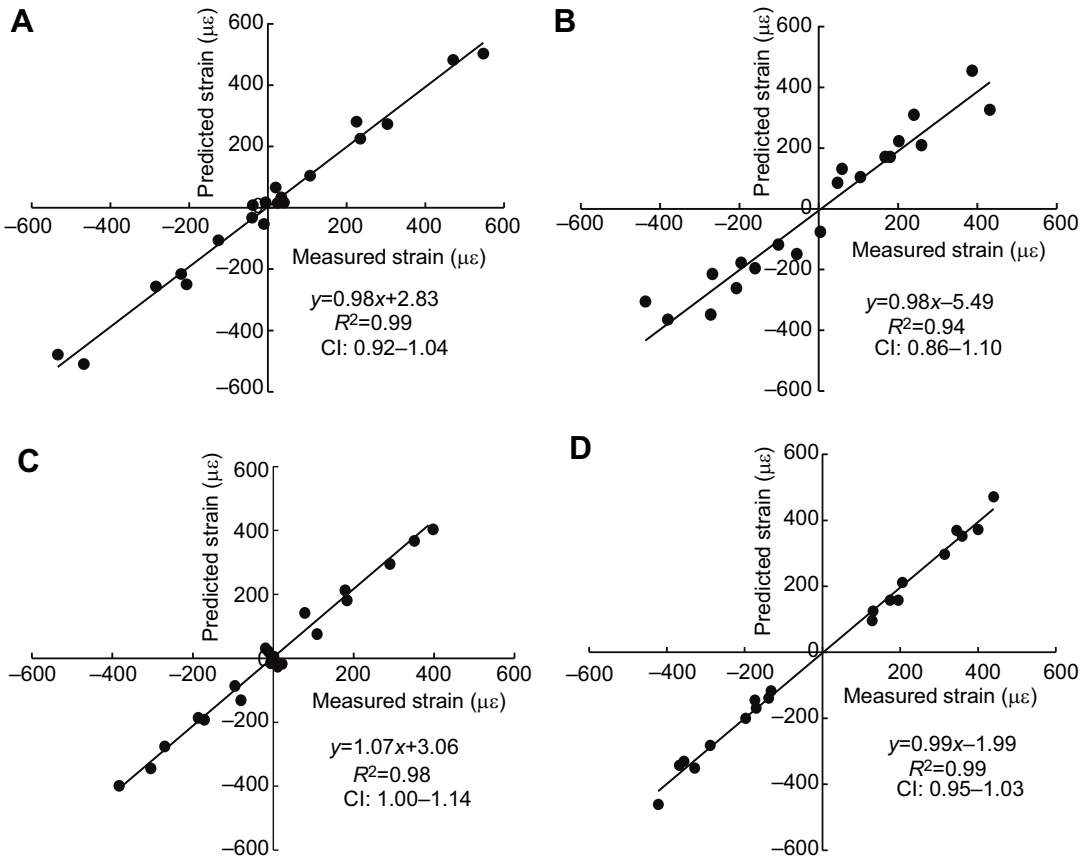


**Fig. 3. Measured versus predicted strain (με) for the different gauge locations.** (A) Anterior gauge site, (B) posterior gauge site, (C) medial gauge site and (D) anterior–medial gauge site. Each plot contains data from all four bending directions such that, for example, in A, strains would be large and positive or negative during posterior and anterior bending, respectively, and close to zero during medial and lateral bending, indicating the gauge site was close to the neutral axis. The line through the data represents the linear regression fit; the slopes, $R^2$ values and 95% confidence intervals (CI) are given in each plot.

and medial bone surfaces, each surface was prepared for gauge attachment by removing an approximately 1 $cm^2$ region of periosteum, lightly scraping the underlying surface with a periosteal elevator, and defatting and drying the surface using 2-butanone (Sigma-Aldrich). Strain gauges were then bonded to each site using a self-catalyzing cyanoacrylate adhesive (DURO Superglue, Loctite). Gauges were centered on each surface as much as possible (Fig. 4, Table 2), and the central element of the rosette was aligned with the long axis of the bone within 5 deg. Once all three gauges were bonded to the TBT, the overlying musculature was carefully replaced and the incisions overlying the hip and TBT were sutured (4-0 coated Vicryl violet braided, J392H, ETHICON, Somerville, NJ, USA). The lead wires exiting over the synsacrum were further anchored to the skin with suture to provide tension relief for the wires, and the incision and the pre-soldered epoxy-mounted connector were covered with gauze and elastic bandaging tape. Following surgery and immediately prior to experimental testing the following day, each bird was given intramuscular injections of analgesic (0.5 mg $kg^{-1}$ meloxicam, VETone, Boise, ID, USA).

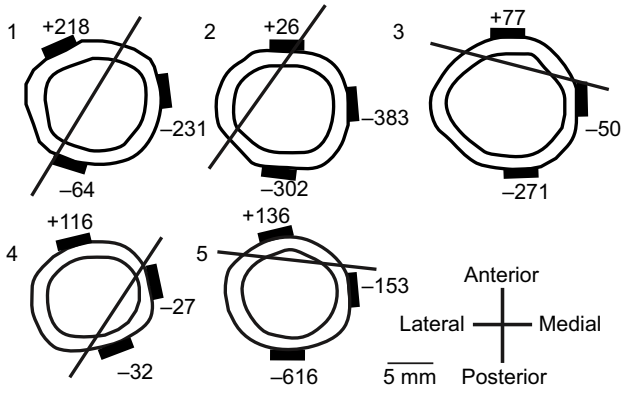


**Fig. 4. Cross-sectional strain distributions for each guineafowl TBT included in this study at the time of peak compressive longitudinal strain on the posterior bone surface.** The strain gauge positions for the five TBT (1–5) are represented by black rectangles. The average longitudinal strain values (με) have been included next to the appropriate gauge. The approximate location of the neutral axis for each animal at the time of analysis is indicated on each cross-section.

**Table 2. Guineafowl subject data and strain gauge positions relative to the bone midshaft**

| | | | Gauge distance from midshaft (mm) | | |
|---|---|---|---|---|---|
| Animal | Mass (kg) | Age (weeks) | Anterior | Posterior | Medial |
| 1 | 2.6 | 21 | –2.0 | –3.1 | –4.8 |
| 2 | 2.9 | 21 | +4.5 | +2.4 | +3.8 |
| 3 | 3 | 21 | –1.5 | –2.3 | –3.9 |
| 4 | 2.8 | 22 | –8.1 | –6.4 | –6.5 |
| 5 | 2.3 | 23 | +5.8 | +2.2 | +2.4 |

For gauge distance, positive values are proximal, negative are distal.

Journal of Experimental Biology (2016) 219, 3082-3090 doi:10.1242/jeb.134536

The day following surgery, *in vivo* bone strain data were collected as the birds ran on a motorized treadmill over a range of speeds, but we only present data collected at the greatest running speed achieved, which was 2.68 m $s^{-1}$. While on the treadmill, the lead wire connector over the hip was connected to a 5.4 m-long shielded cable and the plug–cable connection was secured to the tail feathers with additional elastic bandaging tape. The cable was connected to a Vishay bridge amplifier, from which raw strain signals were sampled by an A/D converter at 2000 Hz. Following data collection, the birds were induced to a surgical plane of anesthesia by mask inhalation of isoflurane (5%) at a 1 l $min^{-1}$ $O_2$ flow rate and then killed via intravenous injection of sodium pentobarbital in the brachial vein (320 mg $kg^{-1}$ Beuthanasia-D, Schering-Plough Animal Health, Union, NJ, USA).

Raw strain data for five consecutive, steady footfalls within each trial for each bird were imported into a custom-written MATLAB program for further analysis. Zero strain levels were determined by averaging the strains during the swing phases of the selected strides. Raw strain data from each rosette were used to calculate principal tensile and compressive strains and the orientation of these strains relative to the long axis of the bone using standard equations that assume a uniaxial planar state of strain (Biewener, 1992):

$$\begin{aligned} E1 &= (\varepsilon_a + \varepsilon_c)/2 + [(\varepsilon_a - \varepsilon_c)^2 + (2\varepsilon_b - \varepsilon_a - \varepsilon_c)^2]^{1/2}/2 \\ E2 &= (\varepsilon_a + \varepsilon_c)/2 - [(\varepsilon_a - \varepsilon_c)^2 + (2\varepsilon_b - \varepsilon_a - \varepsilon_c)^2]^{1/2}/2 \\ \phi &= {}^1\!/_2\,(\tan^{-1}[(2\varepsilon_b - \varepsilon_a - \varepsilon_c)/(\varepsilon_a - \varepsilon_c)]) \\ \gamma &= 2 \times (E1 \times \sin\phi \times \cos\phi - E2 \times \sin\phi \times \cos\phi). \end{aligned} \quad (2)$$

The equation for calculating shear strain ($\gamma$) relies on the calculation of principal tension ($E1$) and principal compression ($E2$), as well as the angle of principal tension ($\phi$). The equations for principal tension, principal compression and the angle of principal tension include contributions from longitudinal strain measures ($\varepsilon_b$) as well as the off-axis components of strain ($\varepsilon_a$ and $\varepsilon_c$) that can all only be experimentally measured simultaneously using a rosette strain gauge.

The time point during stance corresponding to minimum longitudinal strain (peak compression) on the medial surface was chosen for further shear strain analysis in order to guarantee that both posterior and medial gauges were simultaneously measuring compression so that our shear predictions based upon the measured longitudinal strains would not attempt to cross the neutral axis. Shear strains were calculated for each gauge at the relevant time point using Eqn 2 (Biewener and Dial, 1995), and mean values for the five stance phases analyzed per bird were calculated for both the medial and posterior gauges. Based upon these mean values, an individual ratio between posterior and medial longitudinal strain was found for each bird, as well as the ratio between the mean medial and posterior longitudinal strains for all animals. Both ratios were then used to separately predict shear strain values at the posterior gauge site using the mean shear strain value measured for each bird at the medial gauge site (Table 3). Our methods were designed to closely replicate those used previously (Blob and Biewener, 1999; Butcher et al., 2008). Previous use of this approach used experimentally measured shear and longitudinal strains collected at one bone location to project shear strains to a site on the bone where the maximum longitudinal strains were expected to occur based upon the planar strain analysis of longitudinal strains. Because we did not know the location of peak longitudinal strain prior to gauge implantation, and would therefore not have a gauge present at this site to experimentally validate the extrapolation of shear strains from known measures, we had to make predictions from a medial to a posterior location, where we could reliably attach rosette gauges in all birds. Additionally, while similar prior studies used a mean longitudinal strain ratio from all animals in the study (typically $N$=2–4), we also found individual ratios for each animal to highlight the variation within a sample. Thus, the measured shear strain data plotted in Fig. 5 represent the mean shear strain values from the posterior gauge measured over five consecutive stance phases and a single predicted posterior shear strain value for each individual. The predicted shear values are based upon the mean shear strains measured at the medial rosette gauge site and either (i) a mean longitudinal strain ratio for each bird or (ii) a mean longitudinal strain ratio averaged across our five bird sample. Predicted versus measured shear strains for both ratios were plotted and a least squares linear regression fit was applied to each to determine the relationship between measured and predicted shear strain values at the posterior gauge site (Fig. 5). Ninety-five percent CIs were calculated to determine whether the relationships between measured and predicted shear strains were significantly different from unity, recognizing that both variation in the data and sample size affect CI range.

## RESULTS

### Measured versus calculated longitudinal strains

All emu TBTs underwent four-point bending in both directions across the medio-lateral and antero-posterior axes, sequentially placing each of the anterior, posterior, medial and lateral bone surfaces in compressive and tensile strains of varying magnitude.

**Table 3. Guineafowl longitudinal and shear strains measured during treadmill locomotion, individual-specific longitudinal strain multiplier, and shear strain extrapolations to posterior gauge site for both multipliers**

| Animal | Medial longitudinal strain (με) | Posterior longitudinal strain (με) | Individual-specific posterior/medial longitudinal strain ratio | Measured medial shear strain (με) | Measured posterior shear strain (με) | Calculated posterior shear strain (με) | |
|---|---|---|---|---|---|---|---|
| | | | | | | Individual specific | Sample mean |
| 1 | −231 | −64 | 0.28 | −360 | −217 | −100 | −547 |
| 2 | −384 | −302 | 0.79 | −657 | −1000 | −518 | −1000 |
| 3 | −51 | −271 | 5.35 | −159 | −263 | −852 | −242 |
| 4 | −27 | −33 | 1.20 | −179 | −35 | −215 | −273 |
| 5 | −153 | −616 | 4.03 | −118 | −695 | −473 | −179 |

Medial and posterior longitudinal and shear strains are experimentally determined values. The individual-specific posterior/medial longitudinal strain multipliers were found by dividing the posterior longitudinal strain value by the medial longitudinal strain value for each animal. The sample-mean multiplier was determined by dividing the mean posterior strain value by the mean medial longitudinal strain value, and for our sample was 1.52. Calculated (extrapolated) posterior shear strains were then determined by multiplying the measured medial shear strain values by the individual-specific and sample-mean multipliers for each bird.



Journal of Experimental Biology

Journal of Experimental Biology (2016) 219, 3082-3090 doi:10.1242/jeb.134536

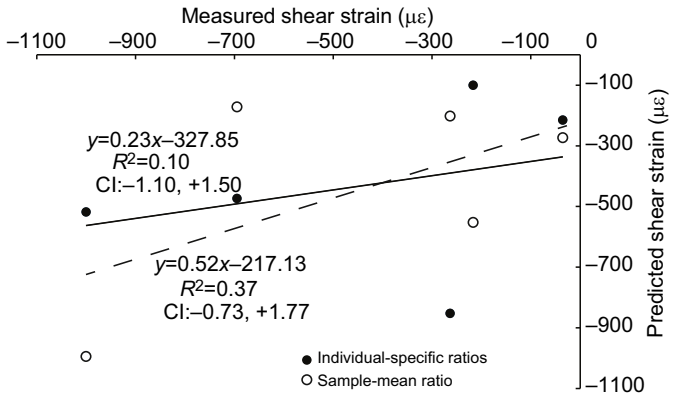


**Fig. 5. Measured versus predicted (extrapolated) shear strain values for each guineafowl for both individual-specific ratios and the sample-mean ratio.** The solid and dotted lines represent the linear regression fits for the individual-specific and sample-mean data, respectively, and the slopes, $R^2$ values and 95% CI are placed closest to their line in the plot.

Strains near zero indicate that the gauge site was close to the neutral axis during bending, as would happen for the anterior gauge site when the upper load points contact the medial or lateral bone surface. For all strain gauge sites, the relationship between measured and calculated longitudinal strains was linear, and the slope of the regression line did not differ significantly from 1.0 as indicated by 95% CIs that included the value 1.0 (Fig. 3). *y*-axis intercept values were all less than 6 με, thus not deviating markedly from the origin. $R^2$ values for anterior, posterior, medial and anterior–medial (single-element gauge) sites were 0.99, 0.94, 0.98 and 0.99, respectively. The percentage of gauge coverage of the bone's circumference during prediction of the anterior, posterior, medial and anterior–medial gauge sites was 47±4%, 32±3%, 55±4% and 70±2%, respectively. This indicates that predictions for the anterior–medial gauge were based upon the broadest gauge coverage of the bone circumference, while predictions for the posterior site were based upon the most restricted gauge coverage of each bone's circumference. Even for the surface with the most restricted gauge coverage, the correlation between measured and predicted strains was strong.

### Extrapolation of planar strain theory to shear strains

Measured shear strains at each rosette gauge and predicted values were analyzed at the time point of the minimum medial axial strain (maximum compression) during stance phase (29±7% through stance) for the five most consistent steps from each trial. Inter-animal variation in gauge position and the approximate location of the neutral axis at the time point analyzed are depicted in Fig. 4. The individual-specific ratios of posterior to medial longitudinal strains (longitudinal strain ratio, Table 3) varied considerably across the different birds (range: 0.28–5.35), indicating that for some birds, posterior longitudinal strains were greater than medial longitudinal strains, while for others the opposite occurred. The causes for this variation can be discerned from the varying strain distributions in the guineafowl TBT (Fig. 4), where for some birds the medial gauge is located closer to the neutral axis (e.g. birds 3 and 4), while for others the neutral axis of bending falls closer to the posterior rosette gauge (e.g. birds 1 and 2). Extrapolated shear strain values using the individual-specific ratio of posterior to medial longitudinal strains resulted in a poor correlation overall between the measured and predicted shear strains at the posterior gauge site. The applied linear fit had a slope of 0.23 ($R^2$=0.10) and an intercept value of −327 με. The sample-mean multiplier (1.52) resulted in a better correlation between measured and predicted shear strains at the posterior gauge site than the individual-specific correlation, with an applied linear fit slope of 0.52 ($R^2$=0.37) and an intercept value of −217 με. However, both multipliers included relationships with slopes equal to 1.0; they also included lines with slopes equal to 0.0. Both the individual-specific and sample-mean ratios produced a positive slope between the measured and predicted posterior site shear strains, which may suggest that, at least for the guineafowl TBT, using this technique could help prevent underestimation of maximal shear strains in the bone.

## DISCUSSION

PST is used in skeletal mechanics studies to predict the distribution of longitudinal strains normal to the bone's transverse cross-section and the location of the neutral axis of bending (Biewener and Dial, 1995; Blob and Biewener, 1999; Butcher et al., 2008, 2011; Lieberman et al., 2004; Main, 2007; Rubin and Lanyon, 1985). To our knowledge, application of this theory to skeletal mechanics has not been experimentally validated. One of our primary goals in this study was to assess the accuracy of PST calculations in matching experimentally measured strain values at several strain gauge sites around a bone's cross-section. We found that predicted strain values closely matched experimentally measured values in long bones loaded in four-point bending. PST has also been used to extrapolate possible peak shear strain values at locations on the bone not instrumented with rosette strain gauges (Blob and Biewener, 1999; Butcher et al., 2008). We sought to test the use of a linear model based upon longitudinal strain measures for predicting shear strains in long bones. Shear strains include contributions from off-axis strain components (Eqn 2) that can only be measured using rosette strain gauges and which may not scale linearly across a bone's cross-section as longitudinal strains do during long bone loading. For our experimental conditions, we found that shear strain values predicted from *in vivo* measures of longitudinal strain generally did not correlate well to experimentally measured shear strain values for the guineafowl. However, both ratios did result in a relationship with a (non-significant) positive slope between the predicted and measured shear strains. Therefore, this technique may help to prevent underestimation of maximal shear strains by predicting increased shear strains with increased longitudinal strains. However, because both positive relationships were non-significant trends, the accuracy of this method could still be questioned.

### PST: longitudinal strain

PST predicts that for an element in bending, longitudinal strains increase linearly perpendicular to the neutral axis of bending. When applied to long-bone biomechanics, this theory assumes that bone material is linearly elastic and isotropic in the transverse plane of section, and has a perfectly cylindrical cross-section (Carter, 1978). If these assumptions are closely matched, longitudinal strain values predicted theoretically at particular sites across the plane of section should equal the experimental strain gauge measures at those same sites. Our results showed that for all four gauge sites sampled, measured and predicted longitudinal strains had a linear relationship not significantly different from unity, with *y*-intercept values less than ±6 με. These data support our hypothesis and the use of PST for predicting bone cross-sectional longitudinal strain distributions when the three gauges required for making longitudinal strain predictions are evenly distributed around the cross-section.

Our data also evaluated the effect of an uneven distribution of gauges in making longitudinal strain predictions. Theoretically, the

Journal of Experimental Biology (2016) 219, 3082-3090 doi:10.1242/jeb.134536

location of the three gauges around the cross-section should not affect predicted strain values. While we found that the linear fit for measured versus calculated longitudinal strains was good for all gauge sites and strain gauge distributions tested, gauge distribution did have a small effect on the confidence of the prediction. Predicted strains for the anterior–medial gauge site had the tightest 95% CI (±0.08) and the greatest percentage of bone perimeter covered (70±2%) by the three gauges used to predict the strains at this fourth gauge site. Predicted strains for the posterior gauge site showed the largest 95% CI (±0.24) and the three gauges used to predict longitudinal strains at this site covered the lowest percentage of bone perimeter (32±3%) of the different gauge combinations examined. Even though surgical accessibility and bone surface limitations often limit gauge placement and distribution around a cross-section during *in vivo* experiments, our results suggest that an even distribution of gauges around the cross-section is not critical when the goal is to model cross-sectional strain distributions using PST. However, predictions made from uneven gauge distributions seem to have slightly more variability. Because the emu TBTs tested here were not solid cylindrical columns of homogeneous bone tissue, results from PST predictions appear to be relatively insensitive to the presence of a marrow canal and the bone tissue heterogeneity likely present in the bones we tested.

The bending moment applied to each bone varied slightly (−8.6 to −10.7 Nm). Because our four-point bending device allows the support points to be adjusted, and they were manually reset between each experiment, the distance between the inner-most and outer-most supports varied (0.10 to 0.12 m), causing slight variations in the applied moment. As our analysis did not depend on achieving specific strain values or specific loads, but rather examined the relationship between strains around a bone's cross-section, the variation in applied moments does not affect our results or conclusions. Theoretically, regardless of the moment applied, longitudinal strains should increase linearly perpendicular to the neutral axis.

PST is often used to evaluate how the *in vivo* strain environment across a bone's cross-section varies during locomotion (Biewener and Dial, 1995; Blob and Biewener, 1999; Main and Biewener, 2004), which typically induces a combination of bending, axial compressive and torsional loads in long bones. We evaluated PST predictions using strain data from bones loaded *ex vivo* in four-point bending, which induces only pure bending. While our results suggest that longitudinal strain predictions closely match the measured strains around a cross-section for pure bending situations, we could not assess the effect of other types of loading combined with bending on the cross-sectional strain distribution and the accuracy of PST predictions in these experiments. Limitations of our mechanical loading system prevented us from applying combinations of bending, compressive and torsional loads to specimens *ex vivo*. Additionally, muscle forces during locomotion could affect the local *in vivo* strain environment, which we could not account for in our *ex vivo* loading model. A valuable future study would include a similar four-gauge analysis conducted *in vivo*. However, as previously stated, *in vivo* gauge attachment is often limited by bone size and surfaces as well as muscle attachment locations. For example, we were not able to perform such a study with the guineafowl TBTs that were used to predict shear strains because there was not an available surface to add a fourth gauge.

### PST: shear strain

Determining the maximum diaphyseal shear strain in a bone during locomotion is also commonly of interest, as shear strain accounts for the off-axis strain components due to torsional and eccentric loading in a bone during locomotion. Just as for longitudinal strains, it is difficult to place a rosette gauge at the location of maximum shear strain without *a priori* knowledge of where peak strains occur around a bone's circumference. Thus, to be able to accurately predict shear strains at non-instrumented locations would be a valuable extension of PST. Attempts have been made to predict shear strains using PST, making the assumption that shear strains increase linearly perpendicular to the neutral axis and in proportion to longitudinal strains. As this approach has been applied to *in vivo* locomotion and *ex vivo* mechanical tests, an average longitudinal strain ratio for the animals used in the study is first determined between measured longitudinal strain values from a rosette gauge located at a similar bone site in each animal, and the longitudinal strain values determined by PST at a non-instrumented location (typically the location of maximum longitudinal strain). Then, the average ratio between the strains at these two sites across all animals in the study is applied to the shear strain measured at each rosette gauge location to produce predicted shear strain values at the non-instrumented locations (Blob and Biewener, 1999; Butcher et al., 2008). However, as shear strains include contributions from off-axis components of strain in addition to longitudinal strain (Eqn 2), it is unclear how accurately the ratio between two longitudinal strain values at different sites around a bone's circumference can be used for predicting shear strains at sites remote to rosette gauge locations.

Our *ex vivo* loading model was not capable of applying the combined axial or bending and torsional loads necessary to create significant shear strain in the bone, so we turned to *in vivo* rosette strain data collected from the guineafowl TBTs during treadmill locomotion to test the accuracy of shear strains predicted using longitudinal strain ratios. At this time we cannot compare the accuracy of our *in vivo* PST-based shear strain predictions with similar *in vivo* locomotor longitudinal strain predictions because we did not have a fourth strain gauge placed *in vivo* for longitudinal strain validation. However, insight into the accuracy of applying PST to shear strain predictions is still important for drawing conclusions from its future use. We did not have *a priori* knowledge of the location of the maximum axial or shear strain at the TBT midshaft in this experiment, so it was not possible to place a rosette gauge at those specific locations to provide empirical data to compare with our predictions. Therefore, we were not able to exactly mimic the methods used previously, where measured shear strains were extrapolated to the site of the predicted peak compressive strains on the bone (Blob and Biewener, 1999; Butcher et al., 2008). However, if the assumption holds that shear strains, like axial strains, increase linearly perpendicular to the neutral axis, then the longitudinal strain ratio should still be able to predict the sub-maximal shear strain values.

Our methods tested extrapolation of shear strains from a rosette gauge site on the medial surface of the guineafowl TBT to a rosette gauge site on the posterior surface. We used both individual-specific and sample-mean longitudinal strain ratios in order to highlight intra-species variation and to more closely mimic previous methods, respectively. We found that for both of the ratios used for shear strain prediction, the predicted versus measured shear strains did not correlate one-to-one linearly with a zero $y$-intercept for the guineafowl in this study. Furthermore, while a slope of 1.0 fell within the CIs for the linear regressions for both ratios used, the intervals themselves were large (−1.10 to +1.50 for individual-specific ratios, −0.73 to +1.77 for sample-mean ratio). There are some limitations in using 95% CIs to distinguish our empirical relationship from an idealized slope, as 95% CIs depend heavily on



Journal of Experimental Biology

sample size. In this case, a linear regression based upon five data points may have led to particularly wide intervals. An increased sample size in future studies could potentially reduce the width of these intervals. Additionally, the individual longitudinal strain ratio between posterior and medial longitudinal strains was both above and below 1.0, depending on the bird, indicating that the location of the neutral axis varied considerably across the birds at the time point used for analysis (when medial longitudinal compressive strains were maximal). We also examined using the time point at which posterior compressive strains were maximal, but this corresponded to positive (tensile) strains on the medial surface for some birds, further indicating the prevalent variation in the neutral axis position and strain distribution present between the individual birds examined. Although it is reasonable to expect greater variation in measured and predicted strain values in a less controlled mode of mechanical loading, such as locomotion, when compared with the highly controlled *ex vivo* bending we used for the PST validation, we would expect a robust method to be able to account for this type of natural variation and still produce a one-to-one linear relationship with a near-zero intercept. Instead, we found non-significant trends that generally showed an increase in predicted shear strain with increased measured shear strain, but also included slopes of zero, indicating no relationship between the measured and predicted shear strain. Measures from additional guineafowl would likely reduce the CIs, perhaps even generating significant trends, which is an important consideration in attempting to evaluate the validity of using this method to predict shear strains in long bone diaphyses. However, the sample size we used here reflects closely the sample sizes typically used in *in vivo* bone strain studies (Biewener and Dial, 1995; Blob and Biewener, 1999; Butcher et al., 2008, 2011; Rubin and Lanyon, 1985). Therefore, the variation present in this sample should be indicative of that seen in studies that would attempt to apply this methodology for estimating shear strains across a bone cross-section.

Table 2 clearly shows inter-individual variation in the medial and posterior axial strain magnitudes, which affects the resultant ratio of these strains and consequently our predicted shear strains. There are several possible contributing factors to the variation in strain magnitudes measured in these birds on the posterior and medial bone surfaces. Although we intended to place the gauges at the bone midshaft and centered on each surface, slight differences in gauge placement around the circumference of the midshaft and/or the proximal–distal position relative to the midshaft were sometimes necessary as a consequence of surface limitations, such as bone size and surface features (i.e. unexpected ridges), which caused us to shift gauge placement slightly (Fig. 4). The greatest difference in proximal–distal gauge placement between any two birds was only about 13.9 mm (−8.1 mm to +5.8 mm from midshaft; Table 2), which only amounts to about 4–6% of the bone's length, and is within the variation described in other *in vivo* strain studies (Main and Biewener, 2007). Additionally, slight differences in bone geometry can affect how load is transmitted through the bone and the resultant strain at a given location. Although none of the animals appeared lame while running on the treadmill, slight differences in running kinematics could easily affect the strain distribution throughout the bone as well. A combination of these factors could have contributed to the inter-individual variation in the neutral axis orientation and location across the birds examined (Fig. 4), which would significantly impact the calculated longitudinal strain ratios for predicting shear strain. However, regardless of the variation in axial and shear strain measures between animals, the predicted shear strains did not closely match the measured shear strains in most of the animals examined here, especially using the individual-specific multiplier. This suggests that the planar relationship between longitudinal and shear strains present in long bones during locomotion does not necessarily correlate one-to-one, at least for the guineafowl TBT.

While our results do not indicate a significant relationship between measured and predicted peak shear strains in the guineafowl TBT, it could be argued that a one-to-one relationship between the measured and predicted shear strains also exists within the variation of our data. Similarly, the generally positive (though non-significant) relationships between the measured and predicted shear strains indicate that predicted strains calculated using a longitudinal strain multiplier could increase in relation to increasing measured shear strains. These two results could be used to argue in favor of applying a longitudinal strain multiplier for prediction of shear strains at non-instrumented sites on a bone surface. Extrapolation of measured shear strains to bone sites of maximal longitudinal strains may help to prevent underestimation of maximal shear strains and, therefore, artificially inflated safety factor estimates (Butcher et al., 2008, 2011). It is also possible that, were this experiment repeated in a different vertebrate taxon, a more consistent relationship could be determined between the measured and predicted shear strains, and the lack of correlation that we found here could be the result of the variability in bone loading seen in the guineafowl TBT (Fig. 4). In some cases the margin of error that PST-based predictions of shear strains may incur might be acceptable given the goals of a particular study, as long as the investigator recognizes the assumptions made and the uncertainty of the results we have found here in attempting to validate this technique. While we found that a one-to-one relationship could be possible between predicted and measured shear strains in the guineafowl TBT, the variation within this relationship also indicates that shear strain predictions using a longitudinal strain multiplier could equally over- or under-estimate the true shear strains occurring at a cortical bone location. If one does hope to apply this methodology, we recommend using a sample-mean-based average longitudinal strain ratio for estimating shear strains as this resulted in a relationship closer to 1.0 and a somewhat tighter CI for the guineafowl TBT, in comparison to the individual-based strain multiplier. However, if a lower margin of error is desired, one should look towards other methods of assessing bone strains at non-instrumented locations, such as finite element analysis (Metzger et al., 2005; Panagiotopoulou et al., 2012; Yang et al., 2014).

In conclusion, PST is a robust and accurate method for predicting the distribution of longitudinal bone strains normal to the cross-section and for determining the location of the neutral axis of bending for bones loaded in *ex vivo* bending. Predicted longitudinal strain values closely matched measured values regardless of the distribution of gauges used for the prediction or the strain magnitudes measured. Repeating a similar analysis with strain data collected during *in vivo* locomotion would further validate the use of this method for bones undergoing more complicated loading regimes than the pure bending examined here. Shear strains measured during *in vivo* locomotion, however, could not be accurately predicted in the guineafowl TBT using longitudinal strain measures. As long as an investigator can accept the potential margin of error present in making shear strain predictions, the method may still have merit for some experiments. However, if more accuracy is desired, alternative methods should be considered. Additional work in several animal species with greater sample sizes would be necessary to attempt to validate a repeatable relationship between longitudinal and shear strain measures in long bones.

**Acknowledgements**
We would like to acknowledge Tony Corsten for his assistance throughout this experiment. We would also like to recognize the Purdue University Research Machining Services for fabricating the potting fixtures, four-point bending apparatus and the alignment frame used during sample potting. We would also like to thank Donna Tudor of the Purdue University Veterinary Teaching Hospital for assistance with obtaining CT images.

**Competing interests**
The authors declare no competing or financial interests.

**Author contributions**
K.A.V., R.P.M. and L.P.L. designed the experiments and test protocols. K.A.V., R.P.M., and M.L. conducted the experimental tests. K.A.V. conducted primary data analysis. K.A.V., L.P.L. and R.P.M. drafted and revised the manuscript.

**Funding**
This work was supported by the National Science Foundation [NSF GRF to K.A.V., DGE-1333468] and The Company of Biologists (JEB travelling fellowship to L.P.L.).

**References**

**Biewener, A. A.** (1992). *In vivo* measurement of bone strain and tendon force. In *Biomechanics – Structures and Systems: A Practical Approach* (ed. A. A. Biewener), pp. 123-147. Oxford: Oxford University Press.
**Biewener, A. A. and Dial, K. P.** (1995). *In vivo* strain in the humerus of pigeons (*Columba Livia*) during flight. *J. Morphol.* **225**, 61-75.
**Blob, R. W. and Biewener, A. A.** (1999). *In vivo* locomotor strain in the hindlimb bones of Alligator *Mississippiensis* and Iguana *Iguana*: implications for the evolution of limb bone safety factor and non-sprawling limb posture. *J. Exp. Biol.* **202**, 1023-1046.
**Butcher, M. T., Espinoza, N. R., Cirilo, S. R. and Blob, R. W.** (2008). *In vivo* strains in the femur of river cooter turtles (*Pseudemys Concinna*) during terrestrial locomotion: tests of force-platform models of loading mechanics. *J. Exp. Biol.* **211**, 2397-2407.
**Butcher, M. T., White, B. J., Hudzik, N. B., Gosnell, W. C., Parrish, J. H. A. and Blob, R. W.** (2011). *In vivo* strains in the femur of the Virginia opossum (*Didelphis Virginiana*) during terrestrial locomotion: testing hypotheses of evolutionary shifts in mammalian bone loading and design. *J. Exp. Biol.* **214**, 2631-2640.
**Carter, D. R.** (1978). Anisotropic analysis of strain rosette information from cortical bone. *J. Biomech.* **11**, 199-202.
**Carter, D., Harris, W., Vasu, R. and Caler, W.** (1981). The mechanical and biological response of cortical bone to *in vivo* strain histories. *Mech. Prop. Bone* **45**, 81-92.
**Lieberman, D. E., Polk, J. D. and Demes, B.** (2004). Predicting long bone loading from cross-sectional geometry. *Am. J. Phys. Anthropol.* **123**, 156-171.
**Main, R. P.** (2007). Ontogenetic relationships between *in vivo* strain environment, bone histomorphometry and growth in the goat radius. *J. Anat.* **210**, 272-293.
**Main, R. P. and Biewener, A. A.** (2004). Ontogenetic patterns of limb loading, *in vivo* bone strains and growth in the goat radius. *J. Exp. Biol.* **207**, 2577-2588.
**Main, R. P. and Biewener, A. A.** (2007). Skeletal strain patterns and growth in the emu hindlimb during ontogeny. *J. Exp. Biol.* **210**, 2676-2690.
**Metzger, K. A., Daniel, W. J. T. and Ross, C. F.** (2005). Comparison of beam theory and finite-element analysis with *in vivo* bone strain data from the alligator cranium. *Anat. Rec. A Discov. Mol. Cell. Evol. Biol.* **283**, 331-348.
**Panagiotopoulou, O., Wilshin, S. D., Rayfield, E. J., Shefelbine, S. J. and Hutchinson, J. R.** (2012). What makes an accurate and reliable subject-specific finite element model? A case study of an elephant femur. *J. R. Soc. Interface* **9**, 351-361.
**Rubin, C. T. and Lanyon, L. E.** (1985). Regulation of bone mass by mechanical strain magnitude. *Calcif. Tissue Int.* **37**, 411-417.
**Yang, H., Butz, K. D., Duffy, D., Niebur, G. L., Nauman, E. A. and Main, R. P.** (2014). Characterization of cancellous and cortical bone strain in the *in vivo* mouse tibial loading model using microCT-based finite element analysis. *Bone* **66**, 131-139.